Statistical shape model of vessel centerline for endovascular paths comparison in mechanical thrombectomy

Aurélien de Turenne[1], Jérôme Szewczyk[2], François Eugène[1],
Anthony Le Bras[1], Raphaël Blanc[3] and Pascal Haigron[1]

Abstract— Endovascular interventions are experiencing an important development. Despite many advantages of this type of intervention, catheter navigation is still a cause of difficulties or failure. Mechanical thrombectomy is one of these interventions where navigation difficulties are related to the ability to navigate the aortic arch and access the carotid. These difficulties are due to the selection of adequate catheters and guides for a specific anatomy and to the technical gesture to operate. The objective of this work is to propose a method to find similar endovascular navigation paths from pre-existing patients to support intervention in mechanical thrombectomy. For each patient, iso-centerlines of the aortic arch and supra-aortic trunks are extracted from pre-operative magnetic resonance angiography volume. A statistical shape model is computed from these vascular structure iso-centerlines. Euclidean distance between vectors of statistical shape model modes is used to compare endovascular navigation paths. A set of 6 patient cases was used to compute the statistical shape model. For validation, an additional set of 5 patient cases was considered to generate new iso-centerlines.
Retrieval of closest iso-centerlines were correct in more than 95% of cases with the proposed method while this percentage goes down to 43% with Euclidean distance between 3D points of iso-centerlines.

Clinical relevance—The presented method allows physicians to retrieve past navigation paths similar to a new one. Used in planning, this could allow to anticipate navigation difficulties in mechanical thrombectomy.

I. INTRODUCTION

Stroke care is of global importance as nearly 800 000 strokes occur in the United States and 1 million in the European Union each year [1]. Mechanical thrombectomy is an endovascular intervention to treat ischemic stroke with great efficacy [2] [3]. For these reasons, mechanical thrombectomy is an intense area of research [4] and innovation [5] [6] [7]. Despite many advantages, catheters navigation can be difficult or impossible upon complex anatomical configurations [8] that leads to intervention failure. The difficulties of navigation reside in the choice of

[1]Aurélien de Turenne, François Eugène, Anthony Le Bras and Pascal Haigron are with the Univ Rennes, CHU Rennes, Inserm, LTSI – UMR 1099, F-35000 Rennes, France (e-mail: aurelien.de-turenne@univ-rennes1.fr; Francois.Eugene@chu-rennes.fr; Anthony.Le.Bras@chu-rennes.fr; Pascal.Haigron@univ-rennes1.fr)

[2]Jérôme Szewczyk is with the Sorbonne Universités, Institut des Systèmes Intelligents et de Robotique, F-75005 Paris, France (e-mail: szewczyk@isir.upmc.fr)

[3]Raphaël Blanc is with the Department of Interventional Neuroradiology, Hôpital de la Fondation Ophtalmologique Adolphe de Rothschild, F-75019 Paris, France (e-mail: rblanc@for.paris)

adequate catheters and guides to select and in the technical gesture to perform [9]. The crossing of the bifurcation from aortich arch to carotid depends from good combination of diagnostic catheter, delivery catheter and guidewire adapted to specific endovascular tortuosity, curvature and torsion. As consequences, navigation difficulties could be apprehended in planning by retrieving similar vascular anatomies leading to similar navigation paths from pre-existing patients who had a mechanical thrombectomy.

Computation of centerlines is a well explored area, in particular for vessel centerlines [10]. Characterization of vascular structures geometries using vessel centerlines has already been reported for liver surgical planning [11] [12] or cerebral aneurysm [13]. Many geometrical properties that are linked to catheter navigation difficulties such as tortuosity, curvature and torsion can be computed from centerlines [13]. Otherwise, statistical shape model (SSM) can be used to capture the morphological variability of a population. This approach is gaining popularity in the biomedical field for diagnosis [14], for decision support process [15] or for data generation [16] [17]. Study of morphological variability of abdominal vascular structures using SSM of centerlines has recently been reported in [18].

The goal of our paper is to propose a simple descriptor of navigation path, based on SSM of vessel centerlines, allowing retrieval of similar paths for planning. This paper is organized as follows: the section II presents the data that are used and presents the proposed method to describe patient's anatomy. Section III presents the results. Finally, Section IV summarizes the conclusions of the research.

II. METHODS

The global approach is given in Fig. 1. First, 3D volumes of vessels are segmented from pre-operative images obtained by magnetic resonance angiography (MRA). Then iso-centerlines are extracted to compute an SSM using singular value decomposition (SVD). For new centerlines, their projection on the SSM gives modes coefficients that are used to compare endovascular paths between them. Finally data are generated for evaluation.

A. Data

For mechanical thrombectomy interventions, pre-operative images can be either MRA or CTA. The routinely used type of images mainly differ from one country to another, in France the standard is to use MRA [19]. The presented study was performed on a set of MRA that consists of
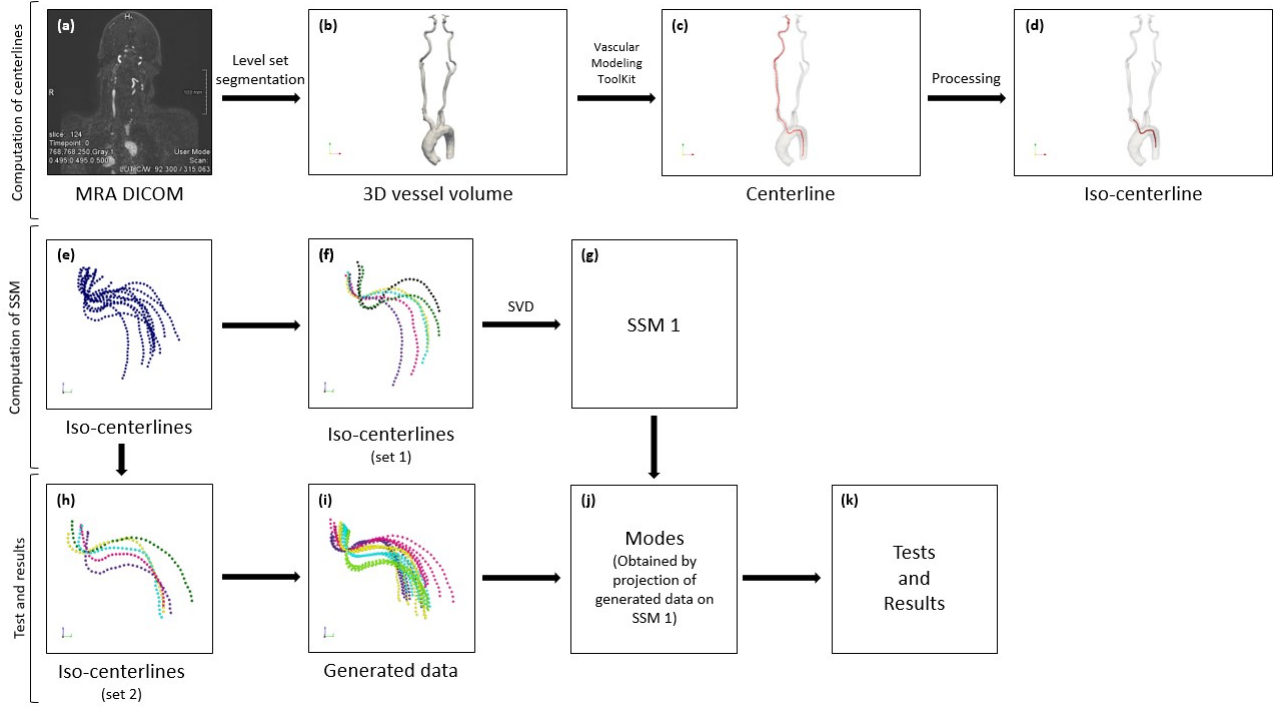
Fig. 1. Overview of the proposed method. From the MRA pre-operative images (a), 3D volumes of vessels (b) are extracted using level set segmentation. From these volumes, centerlines (c) are extracted using the Vascular Modeling ToolKit then the centerlines are resampled, translated and rotated to describe iso-centerlines (d). From the global set of extracted iso-centerlines (e), a first set of 6 centerlines (f) is used to compute an SSM using SVD (g) and a second set of 5 iso-centerlines (h) is used to generate new centerlines (i). These generated centerlines are then projected on the first SSM to get its modes coeffcients (j). Tests are finally realized (k).

11 patients from an observational study for which the data were collected retrospectively at Hopital Fondation Adolphe de Rothschild (Paris, France) from patients who underwent mechanical thrombectomy procedures. Data collection and informed consent form were approved by the local ethics committee. Patients provided written informed consent for the anonymous processing of their data. These 11 patients were aged from 46 to 93 years old with a mean of 76 years old and a standard deviation of 14 years, 8 were female and 3 were male.

B. Segmentation, centerlines extraction and statistical shape model

Regions of endovascular structures were extracted from MRA using level set segmentation [20]. They represent the vasculatures from aortich arch to carotid including the difficult bifurcation (P_{Bif}) to cross using catheters. From these regions, centerlines, featuring vessel geometrical properties such as tortuosity, curvature and torsion (that are linked to endovascular navigation difficulties), are extracted as weighted shortest paths lying on medial axes using the Vascular Modeling ToolKit (VMTK) [20]. Centerlines are then resampled, translated and rotated to describe iso-centerlines. The resampling interval is chosen such that there are 100 equally distributed points between two anatomical points (the bifurcations P_{High} and P_{Bif}) then only points close to the difficult passage are kept: 30 points below and

10 above P_{Bif} (Fig. 2). A translation is applied so that P_{Bif} is at the center of the coordinate system $(O, \vec{x}, \vec{y}, \vec{z})$ and a rotation of center O around $\vec{z}$-axis is applied such that the lowest point of centerline P_{Low} lies in the plane $y = 0$ (Fig. 3) as described in [18].
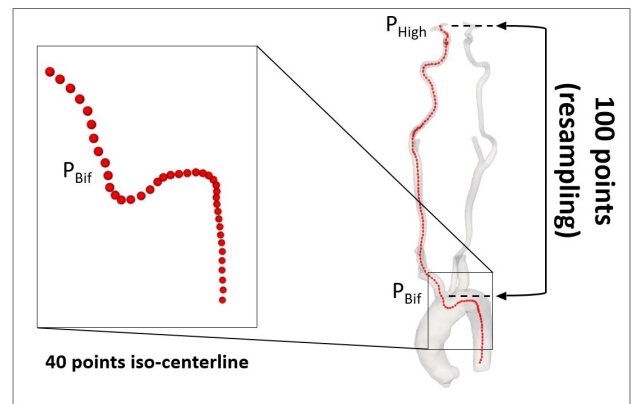

Fig. 2. The resampling interval is chosen such that there are 100 points between P_{High} and P_{Bif}. Only 40 points close to P_{Bif} are kept on resampled centerlines to describe the iso-centerlines: 30 points below P_{Bif} and 10 above.

The centerline of a patient i is represented by the vector L_i. The vector length is equal to 120 that is three times (3D coordinates) the number of points of the iso-centerline (40
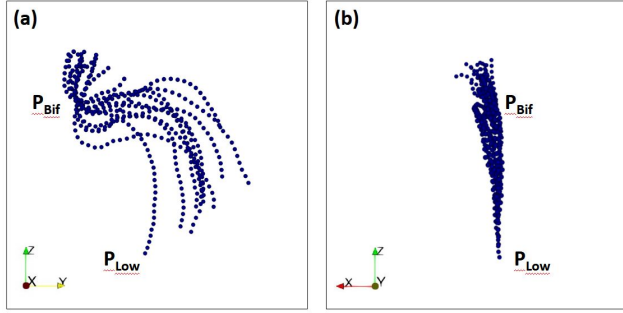
Fig. 3. Iso-centerlines from the set of 11 patients from two different planes. The visualisation in the YZ-plane (a) shows the alignment of the centerlines at P_{Bif} and the visualisation in the XZ-plane (b) shows that P_{Bif} and P_{Low} points lies in the XZ-plane.

points). Using SVD, the matrix composed of the different vectors L_i noted X can be written as:

$$\begin{pmatrix} L_1^T \\ ... \\ L_m^T \end{pmatrix} = X = U\Sigma V^T \qquad (1)$$

where columns of V are the principal directions and columns of $U\Sigma$ are the principal components (or modes).

The descriptor of iso-centerlines is defined as the vector containing the second, third, fourth and fifth standardized modes from the SSM and the distance metric is defined as the Euclidean distance between these vectors.

C. Data generation

In order to evaluate retrieval performance of closest iso-centerlines of the proposed method, different classes of iso-centerlines with similar shapes are required. For this reason, the 11 iso-centerlines are split into two sets: the set 1 (6 patients) in order to compute the SSM from the described method and the set 2 (5 patients) in order to generate new iso-centerlines for validation. Using one iso-centerline from set 2, small variations of this centerline allow to generate new centerlines with a quasi-similar shape. These generated quasi-similar iso-centerlines form a group. Using every iso-centerlines from set 2, it allows to generate 5 groups of 5 quasi-similar iso-centerlines and the presence of five distinguishable groups is visually verified. The groups formed by generated quasi-similar iso-centerlines serve as ground truth. The validation consist in assessing that, given one iso-centerline from one group, the proposed method will retrieve as the four closest iso-centerlines the ones from the same group. Two methods of centerlines generation are used for validation of the proposed method.

a) Method 1: the set 2 of 5 iso-centerlines is used to generate quasi-similar iso-centerlines using weighted arithmetic mean (fig. 4). This first method allows to easily generate new quasi-similar iso-centerlines. Nevertheless, iso-centerlines generated with similar shapes are also spatially close.
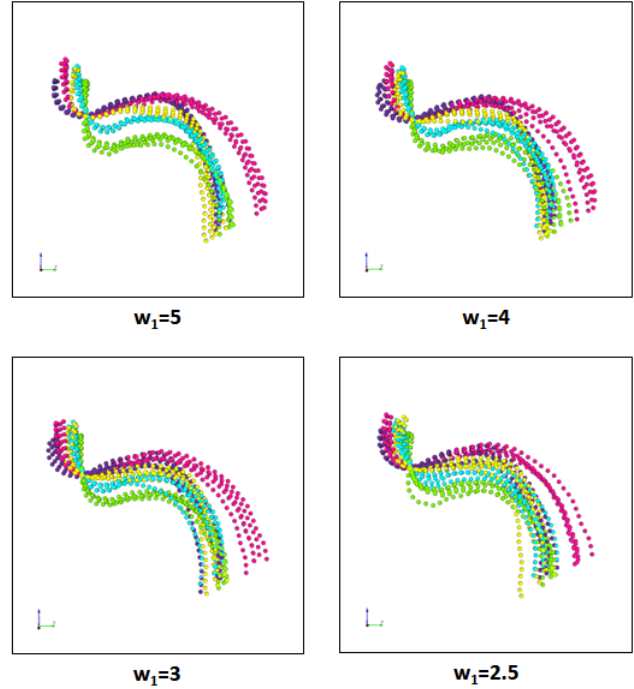

Fig. 4. Generated centerlines with w_1 set to 5, 4, 3 and 2.5: 5 groups of 5 quasi-similar generated CL for each value of w_1.

For one iso-centerline i from set 2, another iso-centerline j from set 2 is randomly selected to compute a new centerline whose k^{th} point can be written as:

$$(x_k^{i(j)}, y_k^{i(j)}, z_k^{i(j)}) = \frac{w_1(x_k^i, y_k^i, z_k^i) + w_2(x_k^j, y_k^j, z_k^j)}{w_1 + w_2} \qquad (2)$$

with w_1 the weight associated to the centerline i (from set 2) and w_2 the weight associated to the another centerline j (from set 2). This operation is repeated 5 times to get 5 quasi-similar iso-centerlines and is applied to every iso-centerlines of set 2 to get the 5 groups of 5 quasi-similar iso-centerlines. The weight w_1 is higher than the weight w_2 such that generated iso-centerlines are close to each other within a group. The value of w_2 was set to 1 and the value of w_1 was set to 5, 4, 3 and 2.5 to get generated groups with different degrees of similarity as shown in fig. 4.

b) Method 2: a set of 5 iso-centerlines (set 2) is used to generate quasi-similar iso-centerlines using an SSM (fig. 5). This second method allows to generate iso-centerlines with similar shapes without being spatially close.

An SSM is computed using the 5 iso-centerlines from set 2. One iso-centerline from this set is projected on the SSM to get its modes then each mode coefficient is modified by randomly (following the uniform law) varying its value by ± Δ%. This operation is repeated 5 times to get 5 quasi-similar iso-centerlines and is applied to every iso-centerline of set 2 to get the 5 groups of 5 quasi-similar iso-centerlines. Centerlines can then be reconstructed using
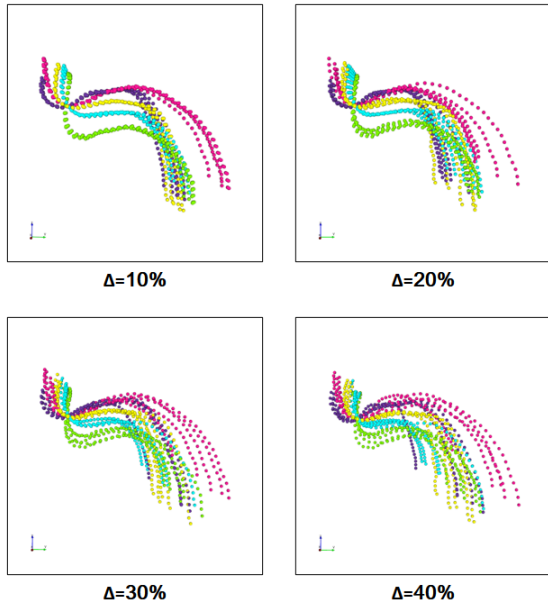
Fig. 5. Generated centerlines with Δ set to 10%, 20%, 30% and 40%: 5 groups of 5 quasi-similar generated CL for each value of Δ.

its modes knowing the principal directions from the SSM. From one centerline i, the coefficient k of the jth generated centerline obtention can be written as:

$$\alpha_k^{i(j)} = \alpha_k^i(1 + \delta_k^{i(j)}) \qquad (3)$$

with $\alpha_k^{i(j)}$ the kth mode coefficient of the jth generated centerline from the ith centerline, α_k^i the kth mode coefficient of the the ith centerline and $\delta_k^{i(j)}$ a random number generated from uniform distribution in the range $[-\Delta, +\Delta]$. The value of Δ was set to 10%, 20%, 30% and 40% to get generated groups with different degrees of similarity as shown in fig. 5.

III. RESULTS

In this section, results of closest iso-centerlines retrieval using the proposed method are presented.

Given a set of 25 generated iso-centerlines (5 groups of 5 quasi-similar iso-centerlines generated from set 2), one iso-centerline from each group is selected and the proposed distance metric (distance between vectors of modes of the SSM computed with iso-centerlines from set 1) is used with each of them to retrieve the four closest iso-centerlines among the set of 25 iso-centerlines. Given one iso-centerline, retrieved iso-centerlines from the same group are considered as correctly retrieved cases. For each value of w_1 (first method of iso-centerlines generation), the presented results are the average of 10 retrieval test with one randomly selected iso-centerline for each group. For each value of Δ (second method of iso-centerlines generation), the results are the average of 10 retrieval test with 10 different sets of 25 generated iso-centerlines with one randomly selected iso-centerline for each group. As shown in the Fig. 6 and Fig.7

(one figure per method used to generate new iso-centerlines), the proposed method gives high percentage of correctly retrieved cases ($> 95\%$) while the Euclidean distance is only efficient when iso-centerlines are spatially very close to each other (high values of w_1 and small values of Δ).
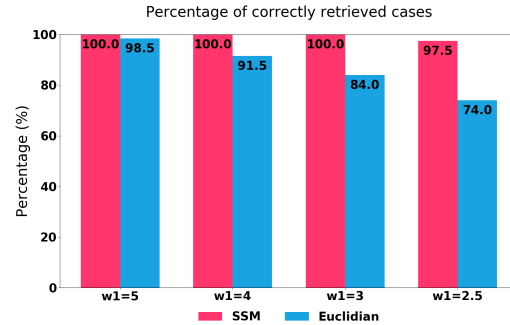

Fig. 6. Percentage of retrieved cases from the same group (correctly classified) using the proposed distance metric (SSM based) compared to a naive distance metric (Euclidian distance between iso-centerlines) on centerlines generated with method 1 (from $w_1 = 5$ to $w_1 = 2.5$).
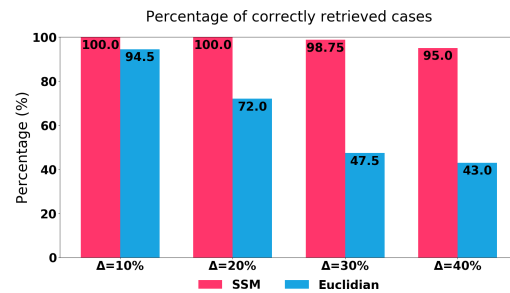

Fig. 7. Percentage of retrieved cases from the same group (correctly classified) using the proposed distance metric (SSM based) compared to a naive distance metric (Euclidian distance between iso-centerlines) on centerlines generated with method 2 (from Δ=10% to Δ=40%).

The results show that the proposed descriptor is able to retrieve similar endovascular paths represented by iso-centerlines (from aortich arch to carotide) to a specific one.

IV. CONCLUSION

We proposed a method for endovascular paths comparison in mechanical thrombectomy. A statistical shape model of vessel centerline from aortich arch to carotid was computed. Modes of SSM were used to compare endovascular paths. Results showed that retrieval of closest cases were correct in more than 95% of cases. For the purpose of planning, this could assist physicians to retrieve endovascular paths from patients already treated to anticipate catheterization difficulties.

ACKNOWLEDGMENT

REFERENCES

[1] Emelia Benjamin, Michael Blaha, Stephanie Chiuve, Mary Cushman, Sandeep Das, Rajat Deo, Sarah de Ferranti, James Floyd, Myriam Fornage, Cathleen Gillespie, Carmen Isasi, Monik Jiménez, Lori Jordan, Suzanne Judd, Daniel Lackland, Judith Lichtman, Lynda Lisabeth, Simin Liu, Chris Longenecker, Rachel Mackey, Kunihiro Matsushita, Dariush Mozaffarian, Michael. Mussolino, Khurram Nasir, Robert Neumar, Latha Palaniappan, Dilip Pandey, Ravi Thiagarajan, Mathew Reeves, Matthew Ritchey, Carlos Rodriguez, Gregory Roth, Wayne Rosamond, Comilla Sasson, Amytis Towfighi, Connie Tsao, Melanie Turner, Salim Virani, Jenifer Voeks, Joshua Willey, John Wilkins, Jason Wu, Heather Alger, Sally Wong, and Paul Muntner. Heart disease and stroke statistics—2017 update: A report from the american heart association. 135(10).

[2] Stephan Munich, Kunal Vakharia, and Elad Levy. Overview of Mechanical Thrombectomy Techniques. *Neurosurgery*, 85(suppl_1):S60–S67, July 2019.

[3] Matthew Evans, Phil White, Peter Cowley, and David Werring. Revolution in acute ischaemic stroke care: a practical guide to mechanical thrombectomy. *Practical Neurology*, 17(4):252–265, August 2017.

[4] Raphaël Blanc, Simon Escalard, Humain Baharvadhat, Jean Philippe Desilles, William Boisseau, Robert Fahed, Hocine Redjem, Gabriele Ciccio, Stanislas Smajda, Benjamin Maier, François Delvoye, Solène Hebert, Mikael Mazighi, and Michel Piotin. Recent advances in devices for mechanical thrombectomy. *Expert Review of Medical Devices*, 17(7):697–706, July 2020.

[5] Markus Johannes Harmen Den. CATHETER TYPE SELECTION. U.S. Patent 20190298278A1, Oct. 3, 2019.

[6] Paul Lucas, Bracken Dr, and Ellicott City. MULTI-FUNCTIONAL THROMBECTOMY DEVICE. U.S. Patent 007645290B2, Jan. 12, 2010.

[7] Thomas Osborne. LOOP THROMBECTOMY DEVICE. U.S. Patent 008361095B2, Jan. 29, 2013.

[8] Martin Werner, Yvonne Bausback, Sven Bräunlich, Matthias Ulrich, Michael Piorkowski, Josef Friedenberger, Johannes Schuster, Spiridon Botsios, Dierk Scheinert, and Andrej Schmidt. Anatomic variables contributing to a higher periprocedural incidence of stroke and TIA in carotid artery stenting: Single Center Experience of 833 Consecutive Cases. *Catheterization and Cardiovascular Interventions*, 80(2):321–328, August 2012.

[9] Dominik Heider, Andreas Simgen, Gudrun Wagenpfeil, Philipp Dietrich, Umut Yilmaz, Ruben Mühl-Benninghaus, Safwan Roumia, Klaus Faßbender, Wolfgang Reith, and Michael Kettner. Why we fail: mechanisms and co-factors of unsuccessful thrombectomy in acute ischemic stroke. *Neurological Sciences*, 41(6):1547–1555, June 2020.

[10] Cemil Kirbas and Francis Quek. A review of vessel extraction techniques and algorithms. *ACM Computing Surveys*, 36(2):81–121, June 2004.

[11] Dirk Selle and Heinz-Otto Peitgen. Analysis of the morphology and structure of vessel systems using skeletonization. *SPIE Medical Imaging*, pages 271–281, San Diego, CA, May 2001.

[12] Dirk Selle, Bernhard Preim, Andrea Schenk, and Heinz-Otto Peitgen. Analysis of vasculature for liver surgical planning. *IEEE Transactions on Medical Imaging*, 21(11):1344–1357, November 2002.

[13] Marina Piccinelli, Alessandro Veneziani, David Steinman, Andrea Remuzzi, and Luca Antiga. A Framework for Geometric Analysis of Vascular Structures: Application to Cerebral Aneurysms. *IEEE Transactions on Medical Imaging*, 28(8):1141–1155, August 2009.

[14] Jan Bruse, Kristin McLeod, Giovanni Biglino, Hopewell Ntsinjana, Claudio Capelli, Tain-Yen Hsia, Maxime Sermesant, Xavier Pennec, Andrew Taylor, and Silvia Schievano. A Non-parametric Statistical Shape Model for Assessment of the Surgically Repaired Aortic Arch in Coarctation of the Aorta: How Normal is Abnormal? In Oscar Camara, Tommaso Mansi, Mihaela Pop, Kawal Rhode, Maxime Sermesant, and Alistair Young, editors, *Statistical Atlases and Computational Models of the Heart. Imaging and Modelling Challenges*, volume 9534, pages 21–29. Springer International Publishing, Cham, 2016.

[15] Bastien Rigaud, Antoine Simon, Maxime Gobeli, Julie Leseur, Loig Duverge, Daniele Williaume, Joel Castelli, Caroline Lafond, Oscar Acosta, Pascal Haigron, and Renaud De Crevoisier. Statistical Shape Model to Generate a Planning Library for Cervical Adaptive Radiotherapy. *IEEE Transactions on Medical Imaging*, 38(2):406–416, February 2019.

[16] Seyed Mousavi, Iman Khalaji, Ali Naini, Kaamran Raahemifar, and Abbas Samani. Statistical finite element method for real-time tissue mechanics analysis. *Computer Methods in Biomechanics and Biomedical Engineering*, 15(6):595–608, June 2012.

[17] Serena Bonaretti, Christof Seiler, Christelle Boichon, Mauricio Reyes, and Philippe Büchler. Image-based vs. mesh-based statistical appearance models of the human femur: Implications for finite element simulations. *Medical Engineering & Physics*, 36(12):1626–1635, December 2014.

[18] Claire Dupont, Christelle Boichon-Grivot, Adrien Kaladji, Michel Rochette, and Pascal Haigron. Statistical shape model of vascular structures with abdominal aortic aneurysm. *Surgetica*, June 2019.

[19] Géraud Forestier, Basile Kerleroux, Kévin Janot, François Zhu, Victor Dumas, Jean-François Hak, Eimad Shotar, Wagih Ben Hassen, Romain Bourcier, Sébastien Soize, Jérome Berge, Olivier Naggara, Hubert Desal, Grégoire Boulouis, Aymeric Rouchaud, R. Hanafi, V. L'Allinec, J.-B. Girot, G. Charbonnier, A. Biondi, F. Gariel, G. Marnat, J. Ognard, J.-C. Gentric, C. Barbier, E. Chabert, P. Lebedinsky, T. Tuilier, P. Thouant, P.-O. Comby, M. Mejdoubi, O. Heck, A. Kastler, V. Chalumeau, J. Caroff, T. Personnic, A. Marchal, C. Bogey, O. Eker, X. Carle, C. Dargazanli, I. Derraz, B. Gory, L. Detraz, J. Sedat, O. Zurlinden, S. Escalard, R. Fahed, A. Guedon, V. Civelli, K. Premat, F. Clarençon, E. Ducouret, N. Raynaud, S. Velasco, P.-F. Manceau, C. Paya, F. Eugene, J. Le Moa, C. Papagiannaki, M. Aggour, M. Bintner, J.-B. Veyrieres, J.S. Richter, R. Pop, A. Consoli, F. Di-Maria, C. Arteaga, J. Darcourt, C. Michelozzi, P. Guedin, D. Herbreteau, and A. Le Bras. Mechanical thrombectomy practices in France: Exhaustive survey of centers and individual operators. *Journal of Neuroradiology*, 47(6):410–415, November 2020.

[20] Luca Antiga, Marina Piccinelli, Lorenzo Botti, Bogdan Ene-Iordache, Andrea Remuzzi, and David A. Steinman. An image-based modeling framework for patient-specific computational hemodynamics. *Medical & Biological Engineering & Computing*, 46(11):1097–1112, November 2008.